Alcohol 100 (2022) 23–30

Contents lists available at ScienceDirect

Alcohol

journal homepage: http://www.alcoholjournal.org/

Photoacoustic imaging for *in vivo* quantification of alcohol-induced structural and functional changes in cerebral vasculature in high alcohol-preferring mice (HAP)

Augustine Meombe Mbolle, Hao Yang, Huabei Jiang*

Department of Medical Engineering, University of South Florida, Tampa, FL 33620, United States

ARTICLE INFO

Article history:
Received 15 February 2021
Received in revised form
3 January 2022
Accepted 4 January 2022

Keywords:
binge drinking
cerebral blood vessels
chronic drinking
high alcohol-preferring mice
low alcohol-preferring mice
photoacoustic tomography

ABSTRACT

Alcohol-induced structural and functional changes were studied *in vivo* by photoacoustic tomography (PAT) of the cerebrovascular system in selectively bred alcohol-preferring mice. High (HAP) and low (LAP) alcohol-preferring mice are replicate lines of mice selectively bred to prefer 10% (v/v) ethanol to water and water to ethanol, respectively, in a free-access two-bottle choice scenario. A cohort of 15 singly-housed alcohol-preferring mice (five HAP mice for the experimental group, five LAP mice for the control group, and five other LAP mice set aside) were given free-access two-bottle choice 10% ethanol (v/v) and water in 50-mL graduated drinking bottles mounted on each of their cages for 4 weeks prior to PAT brain scanning. A daily log of the volume of ethanol consumed over a 24-h period was kept. At the end of the fourth week, blood samples were collected from the HAP mice and blood ethanol concentrations (BECs) were measured to ascertain their levels of ethanol intoxication. The mice were then grouped into five weight-matched pairs of HAP and LAP for comparison purposes, and noninvasive *in vivo* PAT imaging was performed on each weight-matched pair. To mimic a binge drinking paradigm, mice were rearranged into four weight-matched groups of three animals each: an HAP mouse and two LAP mice. For each group, one HAP mouse and one LAP mouse received a 20% ethanol solution via intraperitoneal (i.p.) injection after 24 h of ethanol abstinence, in weight-based doses of 3 g/kg prior to imaging, while the last LAP mouse received a sham i.p. injection. PAT images of the brain were collected for 30 min thereafter. Cerebral vascular diameters for selected vessels of interest were extracted from the PAT images and compared between HAP mice and LAP mice. For the binge scenario, changes in vessel diameter and hemoglobin oxygen saturation were extracted from PAT images and studied over a 30-min duration. Vascular diameter was significantly smaller in HAP mice compared to LAP mice in weight-matched pairs. Hemoglobin-oxygen saturation and vessel diameter dropped more quickly in LAP mice than in HAP mice following a 20% ethanol i.p. injection (3 g/kg), with a 32% reduction in cerebrovascular diameter in a 30-min period. This study demonstrates the effectiveness of PAT in alcohol addiction imaging and diagnosis, and its feasibility in studying alcohol-induced changes in vascular structure and perfusion. It also adds to other bodies of evidence to suggest that the effects of binge drinking are more adverse in occasional drinkers than habitual drinkers.

Published by Elsevier Inc.

Introduction

The current understanding of the neurobiology and pathophysiology of alcohol addiction has been largely due to advancements in imaging studies and technology. Often, the knowledge has been acquired indirectly from rodent models of addiction, owing to their similarities to humans in the manner and route of ingestion of various drugs of addiction. Although rodent models can never perfectly replicate conditions in humans, they allow researchers to easily account for and control genetic and environmental factors that are believed to significantly contribute to the predisposition of alcohol addiction. Thus, they can produce an excellent face validity that enables easy clinical translation (Spanagel, 2017).

Computerized tomography (CT) (Cala, Jones, Mastaglia, & Wiley, 1978; Cala & Mastaglia, 1981) and variants of magnetic resonance imaging (MRI) (Pfefferbaum, Sullivan, Mathalon, & Lim, 1997; Sullivan, Rosenbloom, Lim, & Pfefferbaum, 2000) are currently the

* Corresponding author. ISA 7030A, Department of Medical Engineering, University of South Florida, Tampa, Florida 33620, United States. Tel.: +1 813 974 5253.
E-mail address: hjiang1@usf.edu (H. Jiang).

https://doi.org/10.1016/j.alcohol.2022.01.001
0741-8329/Published by Elsevier Inc.

gold standards for alcohol addiction imaging. While CT is radiation-based, MRI is associated with a huge cost, mostly unaffordable for the often-frequent clinical visits associated with alcohol addiction treatment and rehabilitation. Photoacoustic imaging (PAI) is an emerging hybrid optical imaging modality that relies on optical absorption contrast to visualize tissue structures up to several centimeters deep, with scalable ultrasonic resolution. It does this by detecting outgoing broadband ultrasound signals generated from laser-illuminated biological tissue (Bell, 1880; Oraevsky & Karabutov, 2014). PAI has been proposed as a safe optical imaging approach, and is particularly promising for frequent use situations such as routine clinical and preventive examinations (Sun, Jiang, & O'Neill, 2011). Thus, it could be a candidate for the frequent clinical visits associated with alcohol addiction treatment and rehabilitation. It has also been suggested as an imaging tool to detect functional changes in the brain of small animal models of drug abuse and addiction (Jo & Yang, 2011). There seemingly exists an agreement in the literature on the vasoactive properties of alcohol as well as the etiology and mechanism of brain damage associated with alcohol addiction (Cala et al., 1978; Cala & Mastaglia, 1981; Pfefferbaum et al., 1997; Sullivan et al., 2000), with most studies focusing on deep brain regional damage. Studies on cerebral vasculature (Gundersen, van Wageningen, & Grüner, 2013; Mathew & Wilson, 1986; Newlin, Golden, Quaife, & Graber, 1982) focus more on the alcohol-induced changes in cerebral blood flow and cerebral blood volume. Studies that quantify the alcohol-induced changes in cerebral vascular diameter and functional changes such as hemoglobin oxygen saturation, and those involving photoacoustic imaging, are quite limited or non-existent. The current study thus has a dual aim: 1) to demonstrate the feasibility of PAI in brain imaging and to propose it as a cost effective and safe alternative for alcohol addiction imaging, and 2) to exploit the rich optical absorption contrast differences between oxyhemoglobin and deoxyhemoglobin to noninvasively image alcohol-induced changes in cerebral hemoglobin oxygen saturation and quantify changes in cerebral vascular diameter in high (HAP) and low (LAP) alcohol-preferring mice using PAT. The quantification of vascular diameter from medical images can have far-reaching applications in the diagnosis of pathologies related to diabetes, hypertension, and related cardiovascular disorders, which have direct effects on blood vessels as well as in disease staging. Selected blood vessels of interest (VOI) that supply the mesolimbic brain pathway implicated in alcohol addiction are isolated and compared between HAP mice and control LAP mice based on their diameters. We also quantitatively study how cerebral vessel diameter and hemoglobin oxygen saturation change over a 30-min period following a 20% ethanol intoxication via intraperitoneal injection. Our choice of cerebral vessels is largely due to their roles in supplying blood and oxygen to major brain areas.

Materials and methods

Imaging system

We used a 2D multispectral photoacoustic imaging system shown in Fig. 1. A short-pulse laser beam was generated from a portable fast-tuning Phocus mobile OPO laser system (OPOTEK LLC; Carlsbad, California, United States; pulse width: 7 ns; repetition rate: 20 Hz). A custom-made fiber optic bundle coupled the beam (Ceram Optec GmbH, Germany) through interlocked ports and delivered it to the mouse brain tissue. The fiber bundle had an output end with a large circular aperture (numerical aperture: 0.37) that covered the entire mouse head and provided uniform illumination to the entire brain region. The photoacoustic signals generated were detected by a semi-circular cylindrically focused transducer array with 256 elements (Japan Probe Co. Ltd.; Japan). The array had a radius of 65 mm with a center frequency of 4 MHz and a bandwidth greater than 80%. It was coupled with a custom-made 256 channel data acquisition system, which had an integrated amplifier system with an adjustable gain of 40–91 dB (Photosound Technologies Inc.; Houston, Texas, United States; sampling rate: 40 mega-samples per second; resolution: 12 bits; frame rate: 50 Hz). A 3.0 USB cable transferred the signal to the computer in real time.

For a 20-Hz single-pulse imaging, our system collected one complete frame of data in approximately 0.05 s. A custom-made device of the same length as the array kept track of its focal zone and marked the position of the animal head as well as the depth of imaging for all animals.

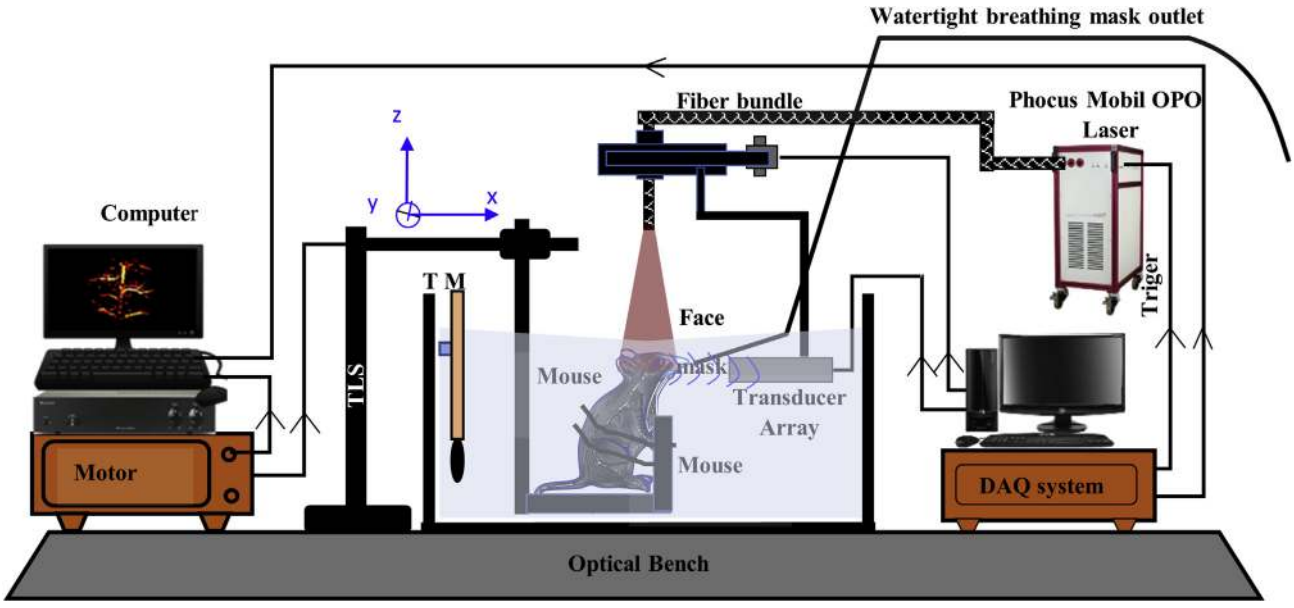

Fig. 1. Photoacoustic imaging system for non-invasive *in vivo* imaging of the cerebral vasculature in alcohol-preferring mice. TM – thermoelectric thermometer with water heater; TLS – translational linear stage.

Table 1
Mean blood ethanol concentration for HAP mice.

Subject (HAP)	S1	S2	S3	S4	S5
Mean BEC (mg/dL)	214.9	220.2	229.1	217.7	233.8
Error (±)	15.55	19.81	13.95	16.55	12.59

By moving the linear stage to which the mouse holder was attached along the z direction, scanning was performed above and below the initial position, to get different planes of the mouse cerebral cortex. A major difference between our imaging system design and traditional PAT imaging systems is the fact that our animals used a custom-made transparent breathing mask fabricated by 3D printing a stereo lithographically formatted model obtained via reverse engineering (Shan, Zhao, Jiang, & Jiang, 2020).

This allowed us to completely immerse the animal holder into water, while supplying life support gases via the inlet and allowing expiration via the outlets. This breathing system was equally used to deliver a low dose of anesthesia, which kept the animal in deep sleep throughout the experiment. Traditional PAT designs place the animal beneath the water tank and use a plastic membrane with ultrasound gel for coupling (Jo & Yang, 2011; Oraevsky & Karabutov, 2014; Sun et al., 2011). Such designs are often associated with acoustic coupling interference issues, which results in artifacts.

Animal model of ethanol dependence and animal handling

The HAP and control LAP mice used in this study were obtained from Indiana University, Purdue University, Indianapolis (Indianapolis, Indiana, United States) (Matson, Kasten, Boehm, & Grahame, 2014; Oberlin, Best, Matson, Henderson, & Grahame, 2011). These are crossed replicate lines of mice selectively bred to prefer 10% (v/v) ethanol over water (HAP) and water over ethanol (LAP). Upon arrival at the University of South Florida (USF), mice were housed in a reversed 12:12-h light–dark cycle colony room, with lights off at 8:00 AM, at the University of South Florida, Department of Psychology (PSY) animal facility. All mice had free access to two-bottle choice 10% ethanol (v/v), water, and rodent chow *ad libitum* for a period of 4 weeks, prior to the imaging experiments. Water and ethanol were provided using 50-mL graduated test tubes mounted on each cage. At the end of the fourth week, blood samples were drawn from the tail at midday when animals were expected to be at peak drinking (Matson & Grahame, 2013; Matson et al., 2014). After plasma supernatant extraction using a Pasteur pipette, blood ethanol concentration (BEC) was measured by means of a benchtop Analox Alcohol Analyzer. This procedure was meant to check that the experimental HAP mice were drinking to intoxication as the daily ethanol consumption data revealed. Table 1 summarizes the BEC data, while Fig. 3 shows the drinking pattern for the best-drinking HAP mice 30 days prior to imaging. Details of the animal model generation and line selection can be seen in these works (Grahame, Li, & Lumeng, 1999; Matson & Grahame, 2013; Matson et al., 2014; Mulligan et al., 2006; Oberlin et al., 2011).

The rodent manipulation procedures were in accordance with a laboratory animal use protocol approved by the University of South Florida Institutional Animal Care and Use Committee (USF-IACUC). All experimental animal procedures were performed in conformity with the guidelines of the US National Institute of Health Guide for the Care and Use of Laboratory Animals (National Research Council of the National Academies, 2011). HAP mice and control LAP mice were paired according to similarity in their weights at the time of imaging, and animals with similar weights were scanned and compared during the same scanning session using the 2D multispectral photoacoustic imaging system described earlier. The animal was affixed to a custom-made mouse holder (Fig. 1) and held in place by loosely tied rubber bands. System settings, including laser energy (12 mJ/cm^2), distance from fiber bundle to animal head (10 cm), as well as the location of the animal's head remained the same from animal to animal. We used a custom-made plastic device to keep track of the head location. After weighing, each animal was administered 4% isoflurane gas anesthesia using an isoflurane anesthetic setup, to induce sleep. While in deep sleep, hair was removed from the scalp region using a rodent clipper and hair removal cream was used afterward to depilate the remaining hair. The breathing mask was then fitted to the mouse face and the tooth bar was used to pull the mouse face until the mask was completely fitted and tight. The oxygen pipe was then connected to the mask's oxygen inlet (Fig. 2). The oxygen flew through 1.0–1.5% isoflurane anesthesia to keep the animal asleep throughout the scanning. Scanning was done with the skull and scalp intact. At the end of the scanning, euthanasia was done with an overdose of isoflurane, followed by cervical dislocation.

PAT imaging of alcohol-induced changes in cerebral vessel diameter

In the first phase of imaging, no additional ethanol was infused into the mice. Our goal was to mimic a free-choice alcohol

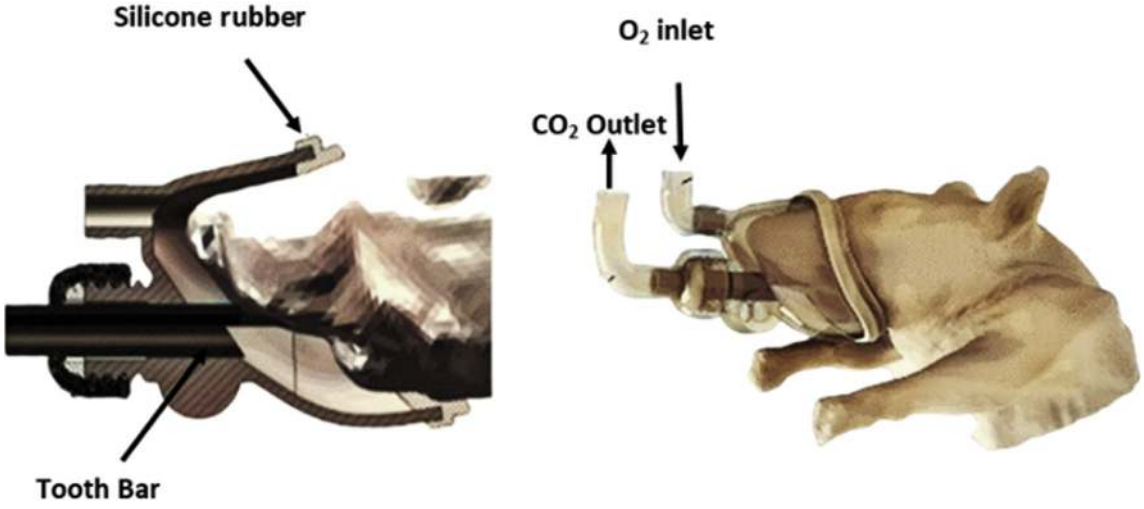

Fig. 2. Illustration of the connection of the mouse breathing mask used to keep the mouse under water for photoacoustic imaging. The silicon rubber seal ensures a tight non-leaky mask.

addiction. Thus, the only ethanol the animals were exposed to was ingested by free choice. For the second phase, mice were arranged into four weight-matched groups of three animals each: an HAP mouse and two LAP mice. For each group, an HAP mouse and one LAP mouse received 145–150 μL of 20% ethanol solution (prepared from ACS grade 190 proof ethanol and sterile 0.9% physiological saline) via intraperitoneal injection (i.p.) after 24 h of ethanol abstinence in weight-based doses of 3 g/kg prior to imaging, while the last LAP received a sham IP injection. The goal was to induce a single ethanol binge (Chen et al., 2013; Ma et al., 2010) and to reduce the variability across subjects observed with ethanol ingestion by free choice (Fig. 3). PAT images were then acquired for 30 min at an isosbestic wavelength of 800 nm, at which the relative photoacoustic signal change reflects the change in total hemoglobin concentration (HbT). Averaging was done at 5-min intervals. Our system's DAQ collects the PAT signal for a single 2D image in 0.05 s, a time shorter than that for one mouse heartbeat. We have neglected heat conduction, since our OPO laser's nanosecond pulse duration is shorter than the thermal diffusion time, to ensure thermal and stress confinement (Sun & Jiang, 2009). Thus, considering only the thermo-expansion mechanism, the photoacoustically generated acoustic field within mouse tissue can be described by the following:

$$\left[\nabla^2 - \frac{1}{c^2}\frac{\partial^2}{\partial t^2}\right] p(r,t) = \frac{\beta}{C_p}\frac{\partial}{\partial t}[\varphi(r)I(t)] \tag{1}$$

where β, C_p, c, $p(\boldsymbol{r}, t)$ and $\varphi(\boldsymbol{r})$ are, respectively, the thermal coefficient of expansion, the specific heat capacity at constant pressure, the speed of sound, the acoustic pressure at position r and time t, and the optical energy absorbed in the mouse tissue. Our goal was to recover $\varphi(\boldsymbol{r})$ from the detected PA signals. We acquired several data frames over a 30-min time span and reconstructed the images using a delay and sum algorithm with temperature-based speed of sound calibration (Hoelen & de Mul, 2000).

Multispectral photoacoustic imaging of alcohol-induced changes in hemoglobin oxygen saturation

For the hemoglobin oxygen saturation imaging, we used the same binge animals as described in Section PAT imaging of alcohol-induced changes in cerebral vessel diameter, and acquired PA signals at 720 nm and 840 nm wavelengths, based on the molar extinction coefficient spectra of oxyhemoglobin (HbO) and deoxyhemoglobin (HbR) (Matcher, Elwell, Cooper, Cope, & Delpy, 1995), using the switchable OPO laser system described earlier. At these wavelengths, HbO and HbR are the predominant optical energy absorbing chromophores with significantly different molar extinction coefficients (Li, Tang, & Yao, 2018). The system collects a single frame of multispectral data in 0.1 s. The laser energy was instantaneously deposited within the mouse cerebral cortex, and assuming invariance in the sound speed and density, the initial acoustic pressure $P_0(\lambda_i, x, y)$ for the i-th (i = 1, 2) wavelength can be thought to represent the reconstructed PAT images $I(\lambda_i, x, y)$ at that wavelength, which itself represents the absorbed energy $E(\lambda_i, x, y)$, but for a constant factor (Li et al., 2018). Our choice of wavelengths (720 nm and 840 nm) around an isosbestic wavelength ensures that the difference $\delta\mu_a$ in absorption coefficients between each image $I(\lambda_i, x, y)$ is small, and that the high sensitivity of our imaging system results in significantly low noise in each of the images $I(\lambda_i, x, y)$ as well as the difference image δI, resulting in negligible uncertainty in sO_2 due to noise. We thus neglected fluence correction (Hochuli, An, Beard, & Cox, 2019). After image reconstruction, we employed a least-square linear spectral fitting technique to obtain the distribution of HbO and HbR (Li et al., 2018). $E(\lambda_i, x, y)$ can be expressed as follows:

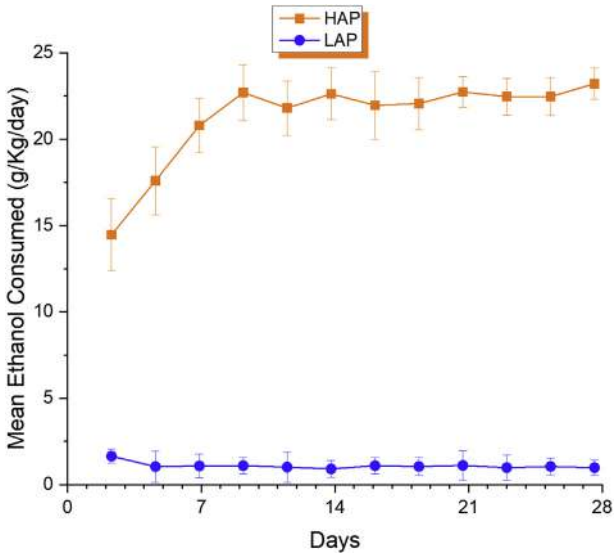

Fig. 3. Mean ethanol consumption per day for HAP and LAP mice. These data are for the five best alcohol drinkers (HAP mice) and the five worst drinkers (LAP mice) used for our imaging experiment. The mice were paired based on their weights for comparison.

$$\begin{aligned} P_0(\lambda_i, x, y) &\cong E(\lambda_i, x, y) = \Phi(\lambda_i)\mu_a(\lambda_i, x, y) \\ &\cong \Phi(\lambda_i)\left(\varepsilon_{\lambda_i}^{HbO_2} C_{HbO_2}^{\lambda_i} + \varepsilon_{\lambda_i}^{HbR} C_{HbR}^{\lambda_i}\right) \end{aligned} \tag{2}$$

where $\Phi(\lambda_i)$ is the fluence and μ_a is the optical absorption coefficient.

From Eqn. (2), the oxygen saturation sO_2 map was calculated as follows:

$$sO_2 = \frac{C_{HbO}(x,y)}{(C_{HbO}(x,y) + C_{HbR}(x,y))} \tag{3}$$

where $(C_{HbO}(x, y) + C_{HbR}(x, y))$ is the total hemoglobin *HbT*.

Results

Extraction and comparison of cerebral vessel diameter in HAP and LAP mice

The significant difference in optical absorption between hemoglobin, deoxyhemoglobin, and the surrounding tissues (Jacques, 2013) results in good contrast, which enables cerebral blood vessels in HAP and LAP mice to be clearly identifiable in PAT images. As shown in Fig. 4A, we extracted the vessels' diameters (strictly speaking, vessel intensity) of the blood vessels by fitting a normalized Gaussian curve, of the form given in Eqn. (4) to a blood vessel's cross-sectional profile along the y direction. Since the Gaussian function never vanishes at the edges, the exact boundaries of the curve cannot be measured directly with exactness. Thus, we have evaluated the full width at half maximum (FWHM) of the Gaussian (Fischer, Uchida, & Messlinger, 2010; Pedersen et al., 2000; Varma, Subramanyan, & Durgan, 2004). It gives the width of the curve at the point where the value of the function is equal to half of its maximum value.

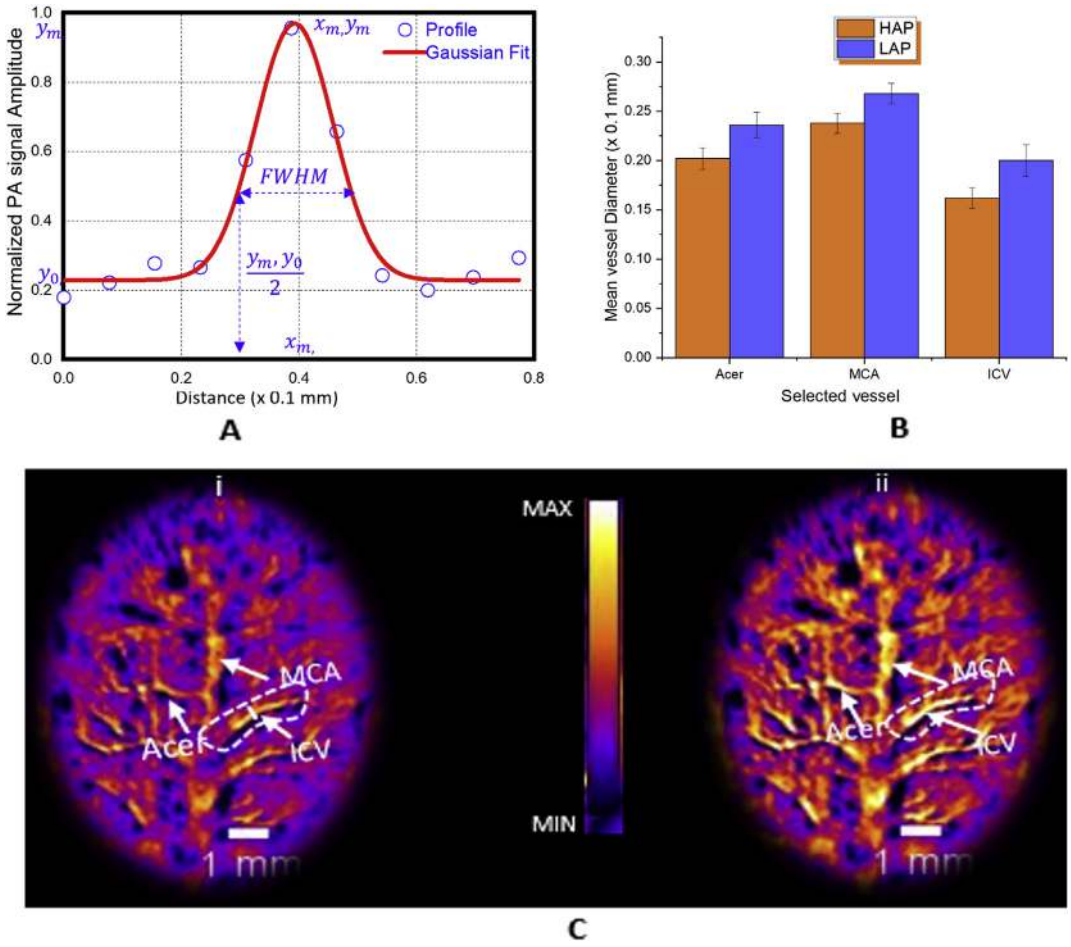

Fig. 4. Estimation and comparison of selected blood vessels between HAP mice and LAP mice. **A**) Details of a normalized Gaussian fit for one of the vessels of interest from which full width at half maximum (FWHM) is estimated (ICV – inferior cerebral vein; MCA – middle cerebral artery; Acer – anterior cerebral artery). **B**) Results of statistical analysis and comparison between selected vessels for five HAP mice and five LAP mice (3 × 5 vessels for each animal model). The error bars indicate the standard deviation in the calculation. With a p value of $p < 0.002$ ($F = 40.38$), the vessels' diameters for HAP mice are significantly smaller than for LAP mice. **C(i)** and **C(ii)**, typical PAT images of HAP and LAP mouse cerebral cortex, respectively, at 800 nm wavelength.

$$y = y_0 + \frac{Ae^{\left(\frac{-(x-x_c)^2}{2\sigma^2}\right)}}{\sigma\sqrt{2\pi}} \tag{4}$$

where $\sigma = \frac{A}{w\sqrt{2\pi}}$ defines the spread of the Gaussian, A is a constant that gives a measure of the PA signal intensity, and w is the full width at half maximum. x_c is the center of the Gaussian, and y_0 is its base.

The Gaussian height y_m occurs at the center where $x = x_c$ and is given by:

$$y_m = \frac{A}{\sigma\sqrt{2\pi}} \tag{5}$$

The full width at half maximum occurs when the Gaussian takes half of its maximum value as shown in Fig. 4A. Upon substitution, rearranging, and solving for $x = w$, we get the full width at half maximum to be:

$$FWHM = w = 2\sigma\sqrt{2\ln 2} \tag{6}$$

which depends only on σ, the spread of the Gaussian.

We then performed a generalized linear model ANOVA on the mean of vessel diameter with animal type as class variable using the SAS software (SAS Institute; Cary, North Carolina, United States) for HAP and LAP, with an α value of 0.005. With a p value of 0.0002, $F = 40.8$, the results show that vessel diameter is statistically and significantly larger in low alcohol-preferring mice, compared to their high alcohol-preferring counterparts. Table 2 summarizes the data.

Estimation of change in hemoglobin oxygen saturation

From the time series images for binge drinking described in Section PAT imaging of alcohol-induced changes in cerebral vessel diameter, we extracted the change in vessel diameter over time for HAP mice and LAP mice. We further extracted the change in hemoglobin oxygen saturation from the multispectral images for HAP mice and LAP mice as described in Section Multispectral photoacoustic imaging of alcohol-induced changes in hemoglobin oxygen saturation and compared the results. Fig. 5A–C shows the oxygen saturation maps over time as well as the comparison of percentage change in vessel diameter and hemoglobin oxygen saturation.

Discussion

We have studied the effect of alcohol dependence on cerebral blood vessels for two drinking paradigms, namely chronic and binge drinking, using photoacoustic tomography (PAT). PAT is an emerging hybrid optical imaging modality that relies on optical absorption contrast to visualize tissue. We have exploited the significant difference in optical absorption between hemoglobin,

Table 2
Summary of vessel diameters for various vessels of interest.

Mice	Vessel (VOI)	Number	Mean Diameter	Standard Deviation	Standard Error	Minimum	Maximum
LAP	MCA	5	0.268	0.010	0.004	0.255	0.280
	Acer	5	0.236	0.013	0.005	0.220	0.245
	ICV	5	0.201	0.015	0.007	0.181	0.220
HAP	MCA	5	0.238	0.010	0.004	0.225	0.244
	Acer	5	0.202	0.011	0.005	0.188	0.215
	ICV	5	0.162	0.010	0.005	0.150	0.175

Acer: anterior cerebral artery; ICV: inferior cerebral vein; MCA: middle cerebral artery.

deoxyhemoglobin, and the surrounding tissues to image and study the direct effects of ethanol on the cerebrovascular system in selectively bred alcohol-preferring mice. HAP mice selectively bred to prefer ethanol to water in a two-bottle free-choice scenario and consume huge amounts of ethanol were used as the experimental subjects. LAP mice selectively bred to consume very little ethanol or no ethanol served as controls. Both animal species belong to the same cohort, were born on the same day, and were bred under the same conditions. Our comparison groups in this study consist of weight-matched HAP and LAP mice. This ensures that we minimize errors that may result from differences in biological clocks in different animals. We have modeled vessel diameter by fitting a Gaussian curve to the cross-sectional profile across the blood vessels. We calculated and equated the Gaussian full width at half maximum (FWHM) to the diameter, which strictly speaking is the vessel's photoacoustic intensity at the point of evaluation. Oxyhemoglobin and deoxyhemoglobin, the proteins responsible for transporting oxygen in blood, are the predominant chromophores

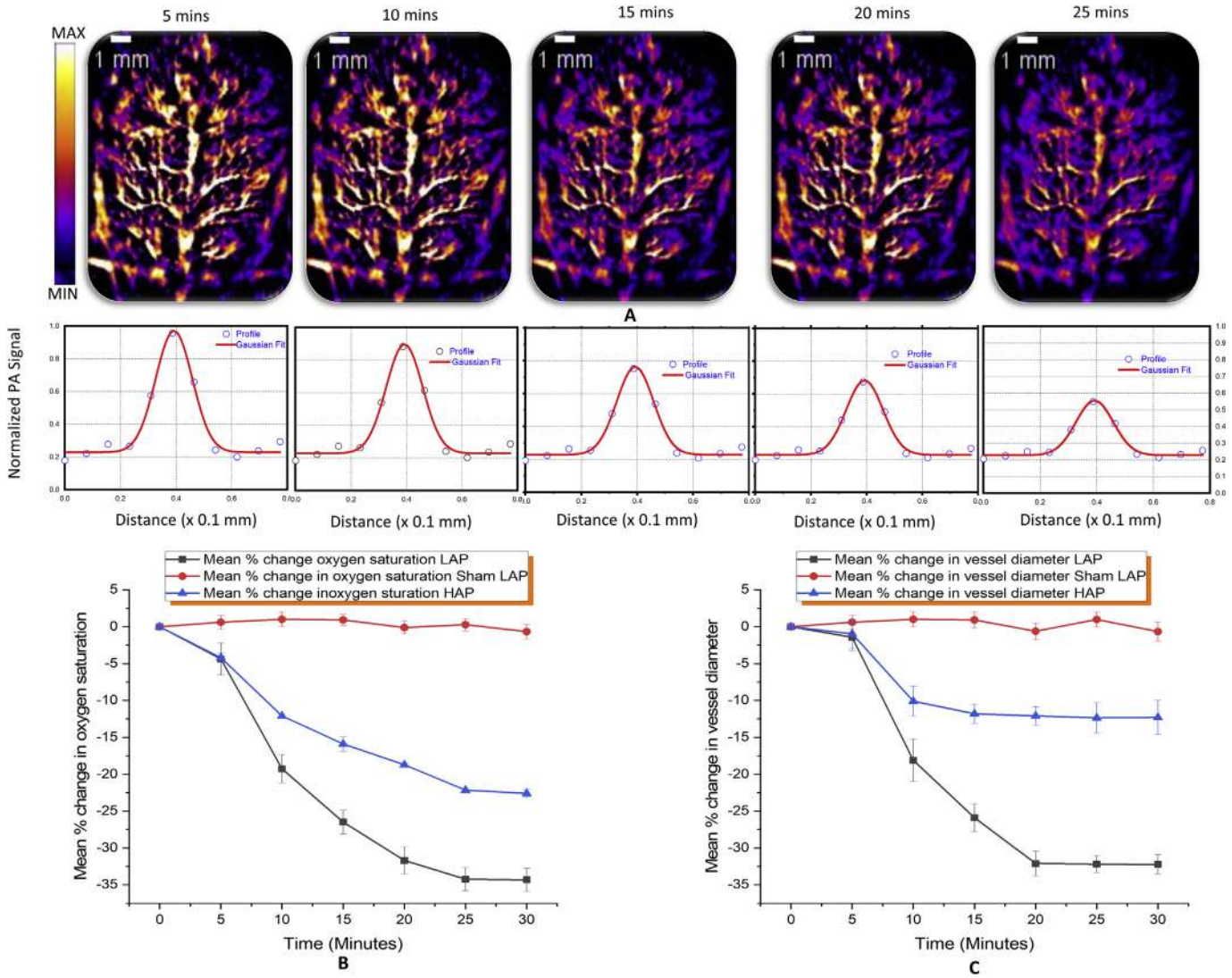

Fig. 5. Estimation and comparison of percentage change in vessel diameter and hemoglobin oxygen saturation with time for a selected vessel between HAP mice and LAP mice when both were acutely injected with 20% ethanol (3 g/kg), after 24 h of ethanol abstinence. **A**) Demonstration of drop in vessel diameter for the selected vessels. **B**) Comparison of the change in vessel diameter for HAP mice and LAP mice. **C**) Corresponding change in hemoglobin oxygen saturation for the same vessel.

that absorb the incident optical energy in this study. Thus, the photoacoustic signal intensity (equivalently the amplitude) is a direct measure of the amount of optical energy absorbed, which indirectly gives a measure of the volume (amount or size) of the absorber or its container (blood vessel). Thus, the alcohol-induced drop in signal intensity for HAP mice, compared to their LAP counterparts, observed in this study is evidence of the drop in container volume/content, namely blood vessel diameter/blood volume. Many other studies have reported such alcohol changes in blood volume (Gundersen et al., 2013; Mathew & Wilson, 1986; Newlin et al., 1982).

The vasoactive properties of alcohol are well known in pharmacology to be dependent on the dose and manner of alcohol consumption. In this study, we used HAP mice that had been made dependent on ethanol at a dose of 10% v/v for their entire life by free choice. We used this unique phenomenon to study the chronic effects of ethanol on cerebral blood vessels by simply imagining and comparing corresponding cerebral blood vessels in HAP and LAP mice of the same weight and age. The LAP mice are genetically bred to consume very little or no ethanol. To study binge drinking and acute alcohol-induced changes in cerebral oxygen saturation, we administered a weight-based dose of 20% v/v ethanol to both HAP and LAP mice, and studied how the vessels' diameter and hemoglobin oxygen saturation changed over time using the functional capabilities of photoacoustic imaging. We then compared the results to weight-matched LAP mice that had received a sham IP injection. This approach reduces the variability in drinking observed with the free-choice drinking and ensures the animals acutely receive a huge dose of ethanol, as in binge drinking.

The exact mechanism of alcohol-induced vascular constriction is not clear in the literature. However, from basic physiology, the major determinant of vascular diameter and thus of resistance and flow rate is the contractile state of the vascular smooth muscle, which is the vascular tone of the vessel. Thus, we have shown using PAT that alcohol exerts its effect directly on vascular smooth muscles to influence their tone. Though blood flow is not strictly laminar, a simple form of Poiseuille's law (Fantini, Sassaroli, Tgavelekos, & Kornbluth, 2016) can be used to model blood flow. The resistance to blood flow can be written as $R = 8\eta L/(\pi r^4)$, where L is the vessel's length, r is its radius, while η and π are constants. The blood flow rate F can be written as $F = (\delta P \pi r^4)/(8\eta L)$, where δP is the pressure difference across a segment of the blood vessel. Thus, vessel diameter has an inverse effect on resistance and a direct effect on flow rate. Therefore, for a given blood volume, vascular constriction results in increased resistance and decreased flow to the brain, resulting in a drop in photoacoustic intensity with time. In particular, the equation shows the dramatic influence vessel diameter has on resistance and flow rate. Blood flow to the brain delivers oxygen used in oxidative metabolism (Bélanger, Allaman, & Magistretti, 2011). Because cerebral neurons are limited in their capacity to undergo anaerobic respiration (Vavilala, Lee, & Lam, 2002), the brain relies on oxidative metabolism for most of its ATP. Thus, blood blow to the brain is crucial for normal brain function. Such alcohol-induced drops in vascular diameter and the resulting resistance to and drop in flow as we have demonstrated could be responsible for acute ischemic stroke (Mostofsky et al., 2010) and aneurysmal hemorrhage reported to be associated with binge drinking, with episodes reported to occur within 24 h of drinking in humans (Altura, Altura, & Gebrewold, 1983). Constriction of vessel diameters observed in this study may also result in such increases in blood pressure reported to be associated with heavy ethanol consumption.

The results from this study show that chronic alcohol dependence is associated with cerebral vessel constriction, as we observed in the HAP mice. Also, binge drinking that involves drinking a huge dose of alcohol at a single instant constricts cerebral vessels as well. More importantly, we have shown that the constriction of cerebral blood vessels and the drop in hemoglobin oxygen saturation following binge drinking is more drastic in occasional binge drinkers, compared to habitual binge drinkers or alcohol addicts. The observed difference in ethanol's effect between HAP mice and LAP mice following a 20% binge ethanol intoxication may result from differences in ethanol tolerance between the two lines of mice. Genetic differences in ethanol metabolism (faster breakdown in HAP mice – more tolerant, due to genetically higher ethanol metabolic enzymes; slower breakdown in LAPs – less tolerant due to genetically fewer ethanol metabolic enzymes) or differences related to adaptation over time, owing to the manner of ethanol consumption (chronic binge in HAP mice, as opposed to episodic binge drinking in LAP mice) between the two lines may account for the observed difference in tolerance.

In conclusion, we have demonstrated the feasibility of using PAT to study changes in vascular structure and perfusion in alcohol addiction imaging and diagnosis. The results show that chronic alcohol dependence is associated with cerebral vascular constriction. Additionally, binge drinking is associated with cerebral vascular constriction and rapid drop in hemoglobin oxygen saturation, with the effect being more drastic in occasional binge drinkers than in habitual binge drinkers. The findings also demonstrate the potential health benefits of identifying and intervening with individuals who binge drink and report tolerance, even when they do not meet current alcohol use disorder diagnostic criteria.

Declaration of competing interest

None.

Acknowledgments

This research was supported in part by internal funds from the University of South Florida.

References

Altura, B. M., Altura, B. T., & Gebrewold, A. (1983). Alcohol-induced spasms of cerebral blood vessels: Relation to cerebrovascular accidents and sudden death. *Science, 220*(4594), 331–333.

Bélanger, M., Allaman, I., & Magistretti, P. J. (2011). Brain energy metabolism: Focus on astrocyte-neuron metabolic cooperation. *Cell Metabolism, 14*(6), 724–738.

Bell, A. G. (1880). On the production and reproduction of sound by light. *American Journal of Science, s3–20*(118), 305–324.

Cala, L. A., Jones, B., Mastaglia, F. L., & Wiley, B. (1978). Brain atrophy and intellectual impairment in heavy drinkers–a clinical psychometric and computerized tomography study. *Australian & New Zealand Journal of Medicine, 8*(2), 147–153.

Cala, L. A., & Mastaglia, F. L. (1981). Computerized tomography in chronic alcoholics. *Alcoholism: Clinical and Experimental Research, 5*(2), 283–294.

Chen, M. M., Palmer, J. L., Ippolito, J. A., Curtis, B. J., Choudhry, M. A., & Kovacs, E. J. (2013). Intoxication by intraperitoneal injection or oral gavage equally potentiates postburn organ damage and inflammation. *Mediators of Inflammation, 2013*, 971481.

Fantini, S., Sassaroli, A., Tgavalekos, K. T., & Kornbluth, J. (2016). Cerebral blood flow and autoregulation: Current measurement techniques and prospects for noninvasive optical methods. *Neurophotonics, 3*(3), Article 031411.

Fischer, M. J., Uchida, S., & Messlinger, K. (2010). Measurement of meningeal blood vessel diameter in vivo with a plug-in for ImageJ. *Microvascular Research, 80*(2), 258–266.

Grahame, N. J., Li, T. K., & Lumeng, L. (1999). Selective breeding for high and low alcohol preference in mice. *Behavior Genetics, 29*(1), 47–57.

Gundersen, H., van Wageningen, H., & Grüner, R. (2013). Alcohol-induced changes in cerebral blood flow and cerebral blood volume in social drinkers. *Alcohol and Alcoholism, 48*(2), 160–165.

Hochuli, R., An, L., Beard, P. C., & Cox, B. T. (2019). Estimating blood oxygenation from photoacoustic images: Can a simple linear spectroscopic inversion ever work? *Journal of Biomedical Optics, 24*(12), 1–13.

Hoelen, C. G., & de Mul, F. F. (2000). Image reconstruction for photoacoustic scanning of tissue structures. *Applied Optics, 39*(31), 5872–5883.
Jacques, S. L. (2013). Optical properties of biological tissues: A review. *Physics in Medicine and Biology, 58*(11), R37–R61.
Jo, J., & Yang, X. (2011). Detection of cocaine induced rat brain activation by photoacoustic tomography. *Journal of Neuroscience Methods, 195*(2), 232–235.
Li, M., Tang, Y., & Yao, J. (2018). Photoacoustic tomography of blood oxygenation: A mini review. *Photoacoustics, 10*, 65–73.
Ma, H., Yu, L., Byra, E. A., Hu, N., Kitagawa, K., Nakayama, K. I., et al. (2010). Aldehyde dehydrogenase 2 knockout accentuates ethanol-induced cardiac depression: Role of protein phosphatases. *Journal of Molecular and Cellular Cardiology, 49*(2), 322–329.
Matcher, S. J., Elwell, C. E., Cooper, C. E., Cope, M., & Delpy, D. T. (1995). Performance comparison of several published tissue near-infrared spectroscopy algorithms. *Analytical Biochemistry, 227*(1), 54–68.
Mathew, R. J., & Wilson, W. H. (1986). Regional cerebral blood flow changes associated with ethanol intoxication. *Stroke, 17*(6), 1156–1159.
Matson, L. M., & Grahame, N. J. (2013). Pharmacologically relevant intake during chronic, free-choice drinking rhythms in selectively bred high alcohol-preferring mice. *Addiction Biology, 18*(6), 921–929.
Matson, L. M., Kasten, C. R., Boehm, S. L., 2nd, & Grahame, N. J. (2014). Selectively bred crossed high-alcohol-preferring mice drink to intoxication and develop functional tolerance, but not locomotor sensitization during free-choice ethanol access. *Alcoholism: Clinical and Experimental Research, 38*(1), 267–274.
Mostofsky, E., Burger, M. R., Schlaug, G., Mukamal, K. J., Rosamond, W. D., & Mittleman, M. A. (2010). Alcohol and acute ischemic stroke onset: The stroke onset study. *Stroke, 41*(9), 1845–1849.
Mulligan, M. K., Ponomarev, I., Hitzemann, R. J., Belknap, J. K., Tabakoff, B., Harris, R. A., et al. (2006). Toward understanding the genetics of alcohol drinking through transcriptome meta-analysis. *Proceedings of the National Academy of Sciences of the United States of America, 103*(16), 6368–6373.
National Research Council of the National Academies. (2011). *Guide for the care and use of laboratory animals* (8th ed.). Washington, DC: National Academies Press. Retrieved from https://grants.nih.gov/grants/olaw/guide-for-the-care-and-use-of-laboratory-animals.pdf.
Newlin, D. B., Golden, C. J., Quaife, M., & Graber, B. (1982). Effect of alcohol ingestion on regional cerebral blood flow. *International Journal of Neuroscience, 17*(3), 145–150.
Oberlin, B., Best, C., Matson, L., Henderson, A., & Grahame, N. (2011). Derivation and characterization of replicate high- and low-alcohol preferring lines of mice and a high-drinking crossed HAP line. *Behavior Genetics, 41*(2), 288–302.
Oraevsky, A. A., & Karabutov, A. A. (2014). Optoacoustic tomography. In T. Vo-Dinh (Ed.), *Biomedical photonics handbook*. Boca Raton, FL: CRC Press.
Pedersen, L., Grunkin, M., Ersbøll, B., Madsen, K., Larsen, M., Christofferson, N., et al. (2000). Quantitative measurement of changes in retina vessel diameter in ocular fundus images. *Pattern Recognition Letters, 21*(13–14), 1215–1223.
Pfefferbaum, A., Sullivan, E. V., Mathalon, D. H., & Lim, K. O. (1997). Frontal lobe volume loss observed with magnetic resonance imaging in older chronic alcoholics. *Alcoholism: Clinical and Experimental Research, 21*(3), 521–529.
Shan, T., Zhao, Y., Jiang, S., & Jiang, H. (2020). In-vivo hemodynamic imaging of acute prenatal ethanol exposure in fetal brain by photoacoustic tomography. *Journal of Biophotonics, 13*(5), Article e201960161.
Spanagel, R. (2017). Animal models of addiction. *Dialogues in Clinical Neuroscience, 19*(3), 247–258.
Sullivan, E. V., Rosenbloom, M. J., Lim, K. O., & Pfefferbaum, A. (2000). Longitudinal changes in cognition, gait, and balance in abstinent and relapsed alcoholic men: Relationships to changes in brain structure. *Neuropsychology, 14*(2), 178–188.
Sun, Y., & Jiang, H. (2009). Quantitative three-dimensional photoacoustic tomography of the finger joints: Phantom studies in a spherical scanning geometry. *Physics in Medicine and Biology, 54*(18), 5457–5467.
Sun, Y., Jiang, H., & O'Neill, B. E. (2011). Photoacoustic imaging: An emerging optical modality in diagnostic and theranostic medicine. *Journal of Biosensors & Bioelectronics, 2*, 108.
Varma, J. K., Subramanyan, K., & Durgan, J. (2004). Full width at half maximum as a measure of vessel diameter in computed tomography angiography. *Proceeding of the SPIE, 5372*, 447–454.
Vavilala, M. S., Lee, L. A., & Lam, A. M. (2002). Cerebral blood flow and vascular physiology. *Anesthesiology Clinics of North America, 20*(2), 247–264.